Supplementary Information

Acoustic Cell Patterning Reveals Geometry- and Substrate-Dependent Vasculogenesis and Human Embryo Model Development

Zhaoyi Xu, [1,§] Weiping Li,[2,3,§] Xufeng Xue,[1,#] Nicholas G. Schott,[2] Chenjun Shi,[3] Ruxin Yang,[1] Shiyu Sun,[1] Jeyoon Bok,[1] Jitao Zhang,[3] Jan P. Stegemann,[2] Jianping Fu,[1,2,4*] Cheri X. Deng[1,2,3*]

Supplementary Movies

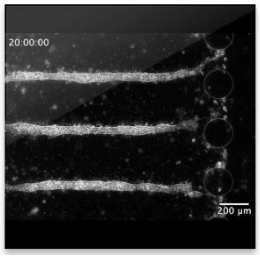

Supplementary Movie 1: Live cell imaging for 1.5 days after acoustic cell patterning (ACP) within a microfluidic device capturing the formation of tubule structures from patterned human pluripotent stem cells (hPSCs).

Supplemental Code 1: COMSOL model for simulation of acoustic pressure and acoustic radiation force acting on a cell within the dish during ACP.

Supplementary Figures

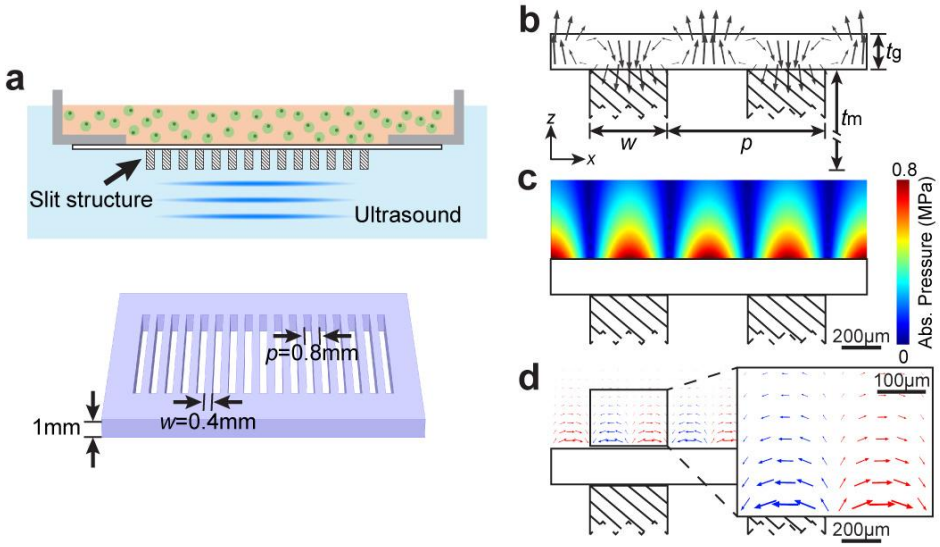

Figure S1. **a**. Schematics of contact-less ACP using ultrasound wave transmitted through a typical 3D printed plate structure (right) placed underneath a glass-bottom cell culture dish. **b.** The particle displacement within the glass slide (thickness t_g) above a 3D printed slit structure (thickness t_m) induced by an incident ultrasound wave. The slit structure has a width of p-w, and p is the period of the slits. **c.** The absolute value of the secondary acoustic pressure field generated in ACP using a slit structure in (**b**). **d**. The acoustic radiation force (ARF) generated by the secondary acoustic field on a spherical cell (diameter 20 µm, speed of sound 1480 m/s, density 1005 kg/m^3).

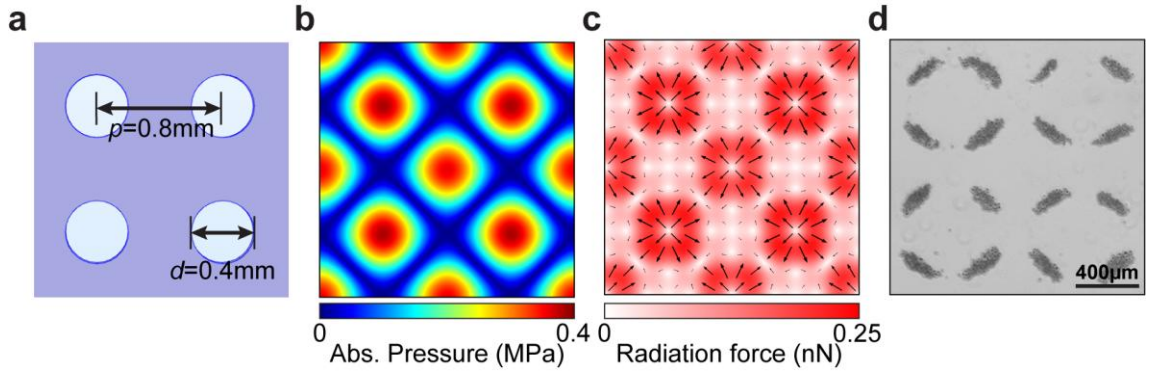

Figure S2. **a**. Schematic of the hole structure with structural dimensions. **b**. Simulated secondary acoustic pressure field (absolute value) generated within a glass-bottom cell culture dish in ACP using the hole structure in (**a**). **c**. The acoustic radiation force (ARF) field generated on a spherical cell using the hole structure (**a**) in ACP showing the direction and amplitude and ARF. **d**. Bright field image of the 2D pattern of normal human lung fibroblasts (NHLFs) (cell seeding density 1M cells/ml) generated using ACP using the hole-structure in (**a**). Acoustic pressure 0.2 MPa. Frequency 1.68 MHz. ACP for 10 s.

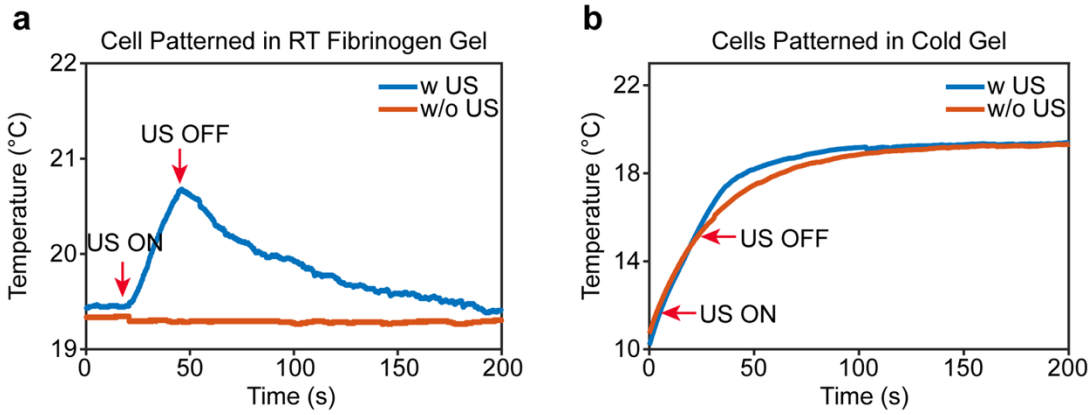

Figure S3. Infrared (IR) measurement of temperature increase with and without ultrasound (US) application in ACP. **a**. Temperature vs. time measured in hPSCs embedded in fibrinogen gel at room temperature (RT). **b**. Temperature vs. time for hPSCs in cold extracellular matrix (ECM) (ice) brought to RT at t = 0 s. For ACP: acoustic pressure 0.14 MPa, frequency 1.68 MHz, application duration 30 s.

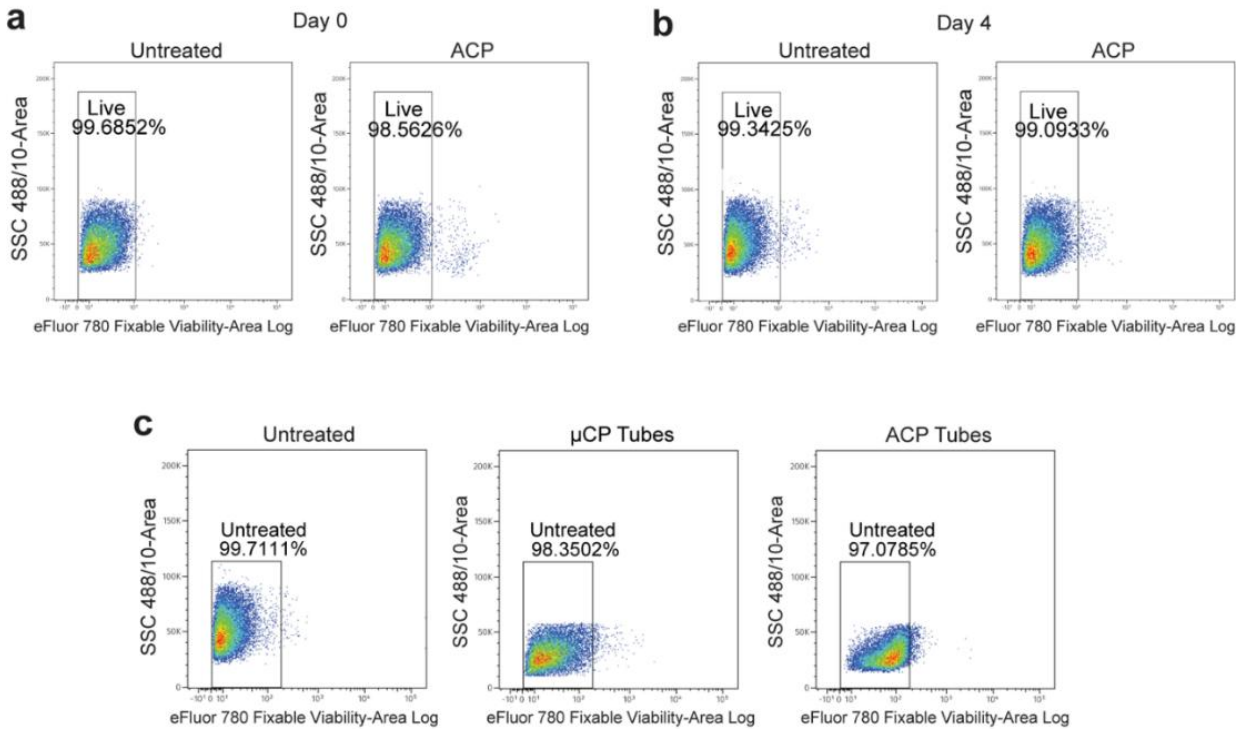

Figure S4. Live/dead assay of cells with and without ACP treatment analyzed using flow cytometry. ACP application was for 60 s and cells were collected (**a**) immediately for analysis or (**b**) after continuous culture in mTeSR for 4 days post-treatment. **c.** Live/dead assays of untreated cells and patterned cells using ACP or microcontact printing (µCP), on day 4. n = 3 independent experiments. For gating strategies, unstained live cells and stained dead cells are used as controls. Cells stained only with viability dye. Debris was excluded by gating the primary cell population on an FSC-A versus SSC-A plot, removing small debris and non-cellular events based on size and granularity.

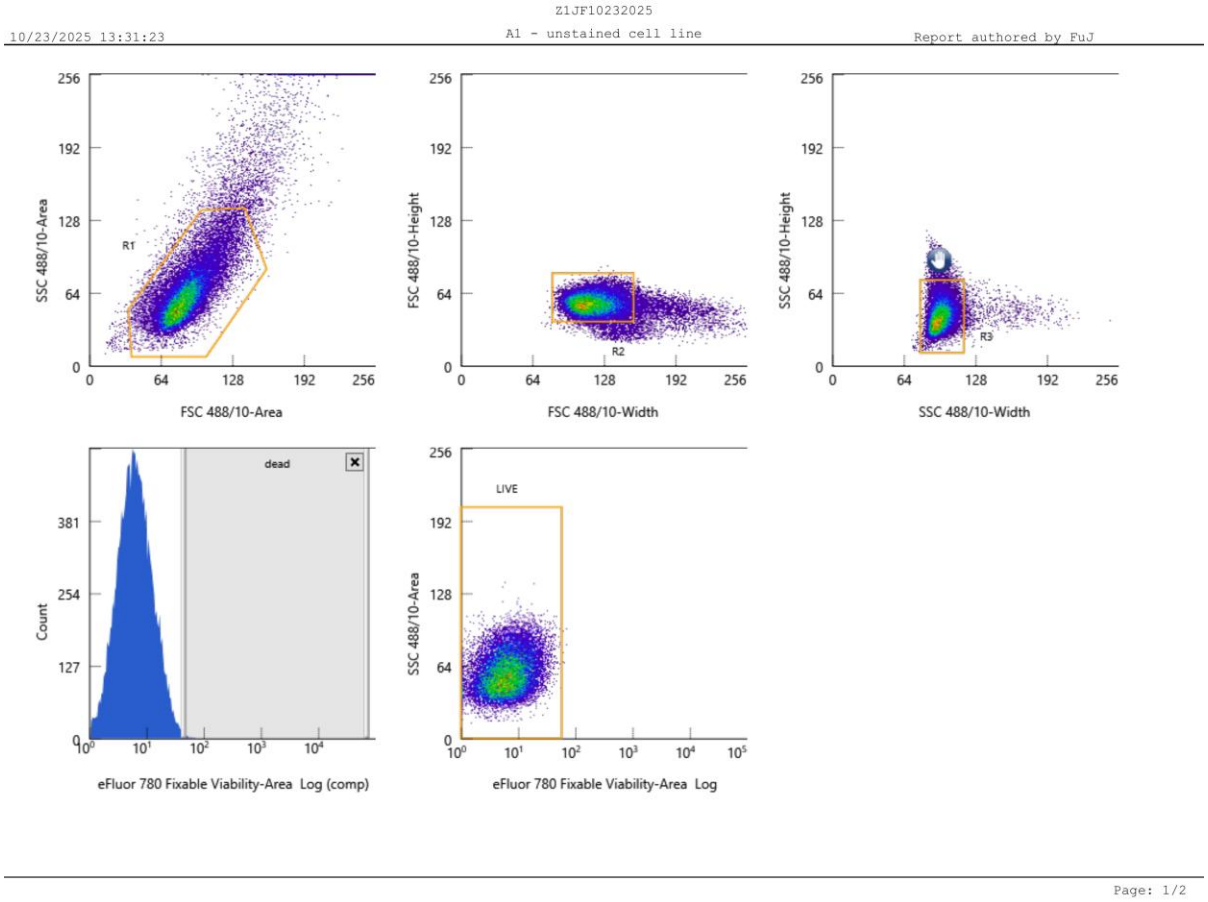

Figure S5. Sample A1, unstained cell line. Top row: the R1 scatter gate on forward-scatter area versus side-scatter area, followed by the R2 and R3 singlet gates on forward- and side-scatter width versus height. Bottom row: the eFluor 780 viability histogram with the dead threshold indicated by the shaded region, and side-scatter area versus viability signal showing the LIVE gate. Of 27,848 events acquired, 19,321 (69.4%) were retained as R3 singlets, of which 15 events (0.08%) fell in the dead gate. As this sample carries no viability dye, its dead fraction defines the background of the measurement and confirms that the threshold is not misplaced into the negative population.

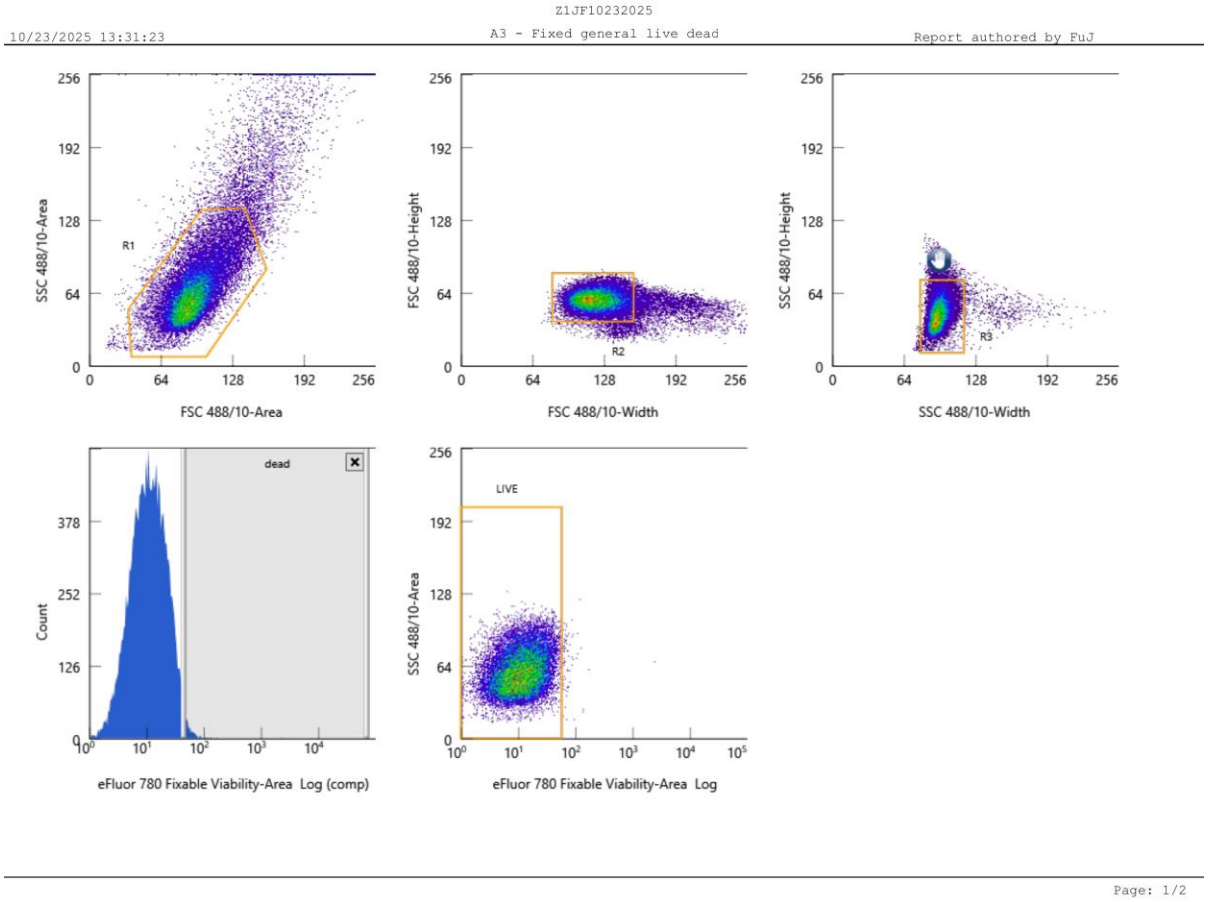

Figure S6. Sample A3, fixed general live/dead control, displayed as in Figure 1. Of 29,018 events acquired, 19,602 (67.6%) were retained as R3 singlets, of which 172 (0.88%) fell in the dead gate. This sample serves as the staining and fixation control against which the treated samples are compared.

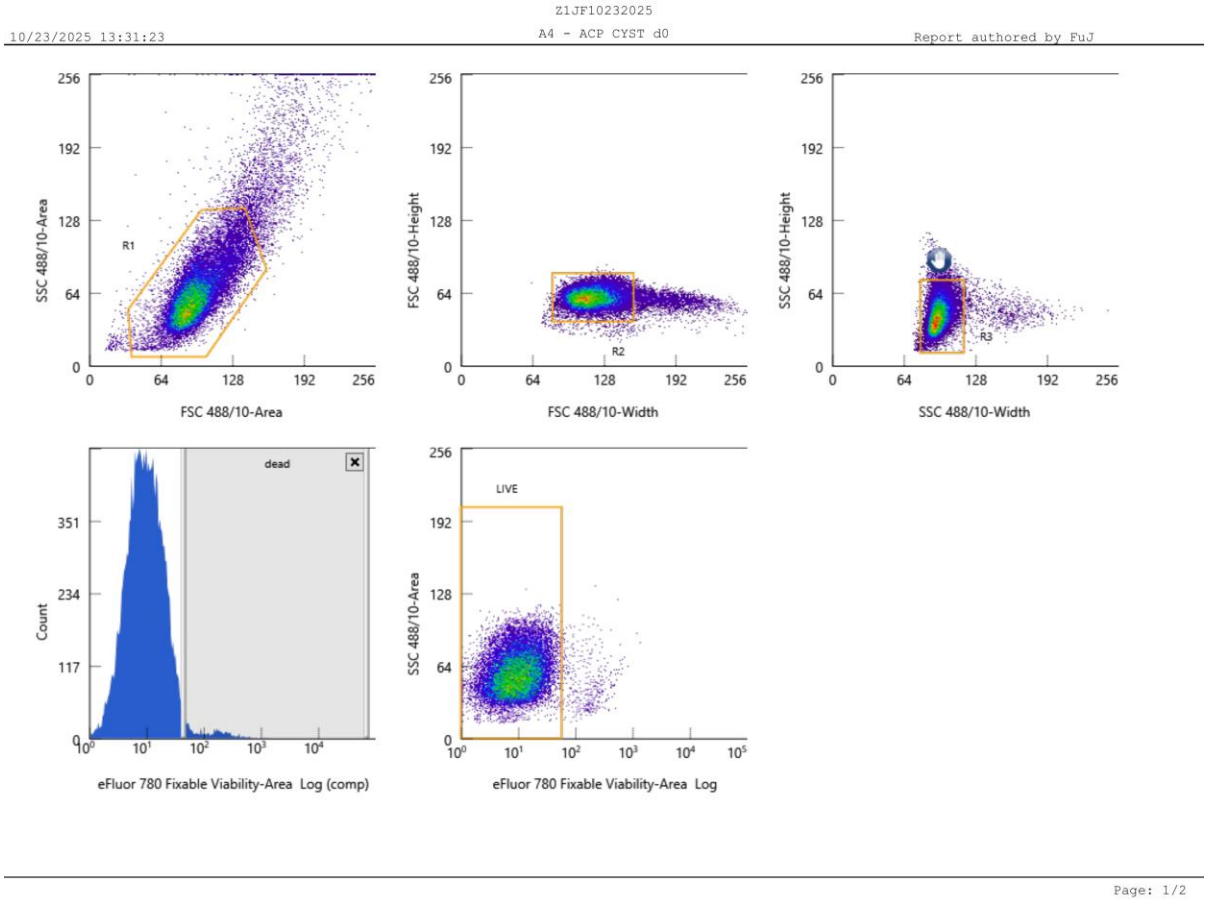

Figure S7. Sample A4, ACP CYST at day 0, displayed as in Figure 1. Of 27,195 events acquired, 20,122 (74.0%) were retained as R3 singlets, of which 464 (2.31%) fell in the dead gate. This is the baseline time point for the ACP CYST condition, measured immediately after treatment.

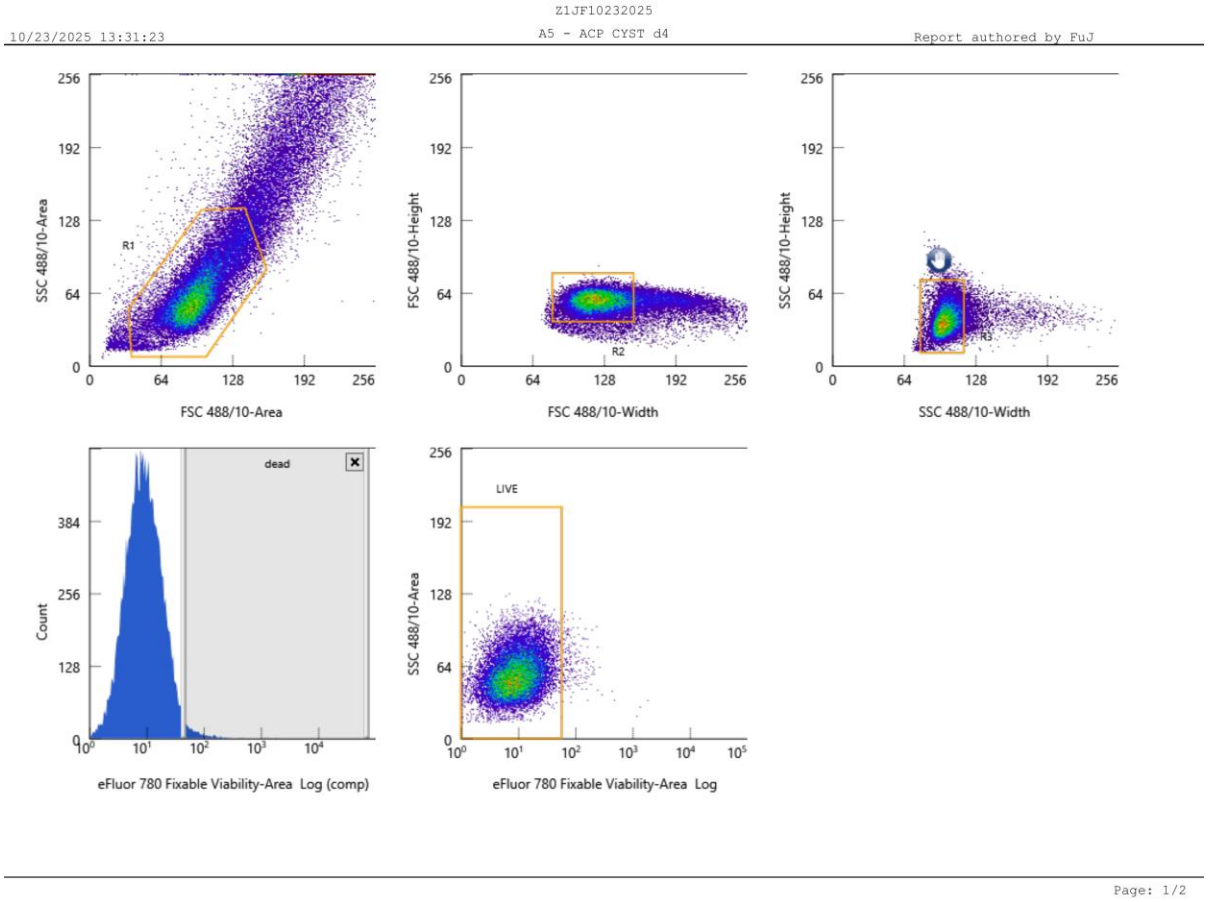

Figure S8. Sample A5, ACP CYST at day 4, displayed as in Figure 1. Of 52,130 events acquired, 19,747 (37.9%) were retained as R3 singlets, of which 283 (1.43%) fell in the dead gate. The dead fraction is lower than at day 0 (Figure 3), indicating that the population did not lose viability over the four-day interval.

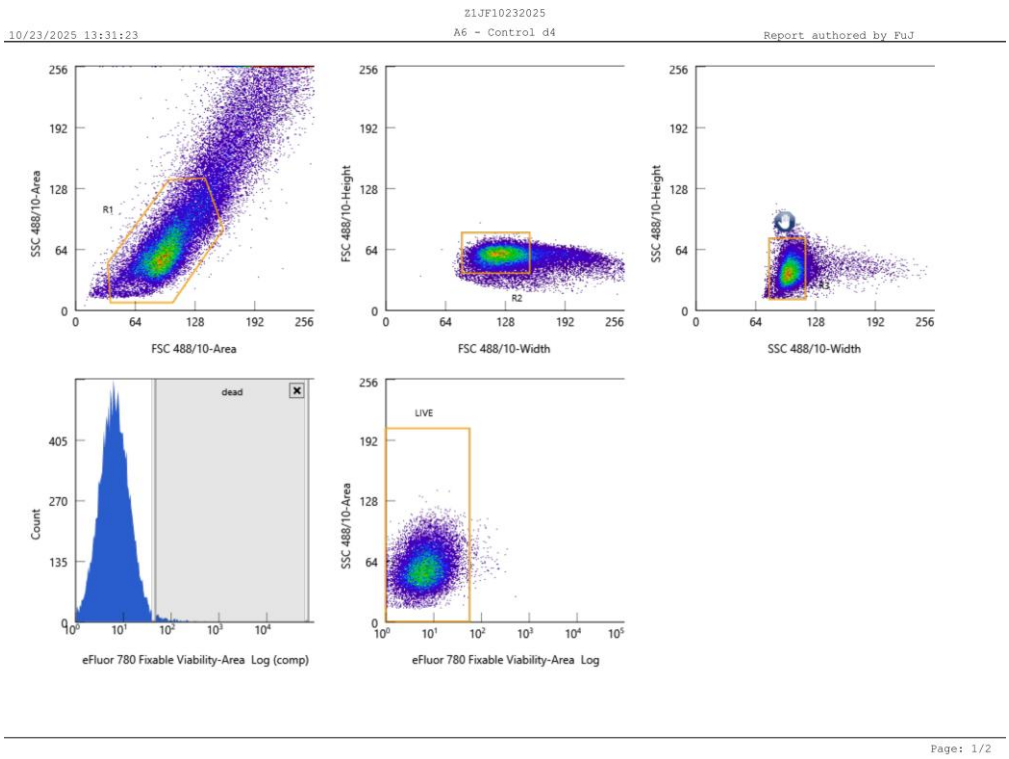

Figure S9. Sample A6, untreated control at day 4, displayed as in Figure 1. Of 50,083 events acquired, 19,748 (39.4%) were retained as R3 singlets, of which 175 (0.89%) fell in the dead gate. This sample provides the reference viability for the day-4 time point.

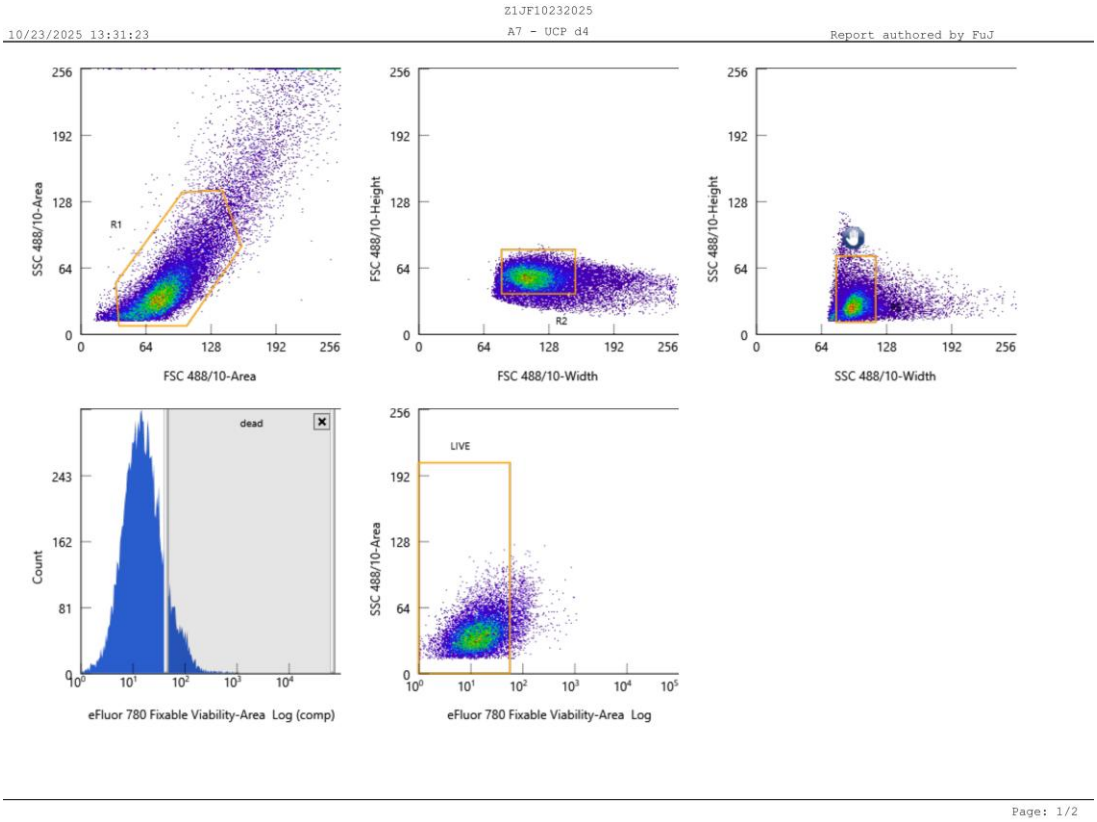

Figure S10. Sample A7, UCP at day 4, displayed as in Figure 1. Of 29,840 events acquired, 14,264 (47.8%) were retained as R3 singlets, of which 1,490 (10.45%) fell in the dead gate. Two features distinguish this sample from all others. First, the viability histogram shows a pronounced shoulder extending into the dead region rather than the single narrow negative peak seen elsewhere, and this shoulder is visible directly in the raw distribution rather than only in the gated statistics. Second, the proportion of acquired events surviving the scatter and singlet gates is markedly lower than in the other day-4 samples, 47.8% against 37.9–39.4% of a much larger acquisition, which is consistent with an increased burden of debris and damaged cells.

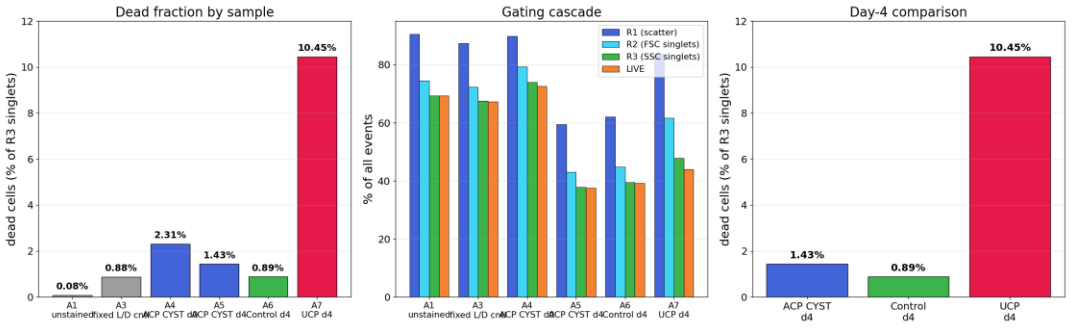

Figure S11. Summary of the gating statistics across all six samples. Left: dead cells as a percentage of the R3 singlet population, with the two control samples in grey. Centre: the gating cascade, showing the percentage of all acquired events surviving each successive gate, R1, R2, R3

and finally LIVE; the difference in overall retention between samples reflects differences in debris content and in the number of events acquired. Right: the three day-4 conditions compared directly. The UCP condition shows a dead fraction of 10.45%, approximately twelvefold that of the day-4 control (0.89%) and sevenfold that of ACP CYST at day 4 (1.43%).

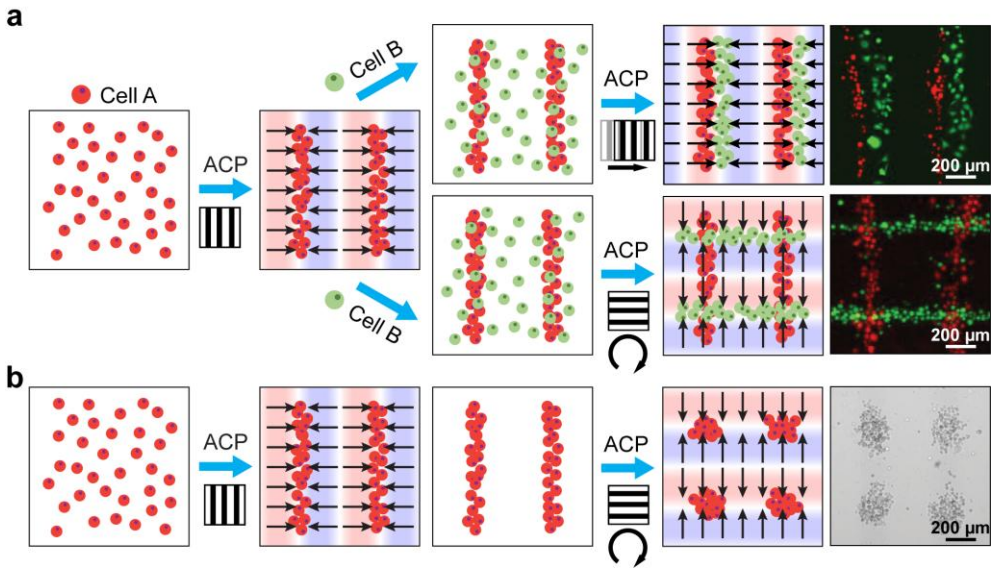

Figure S12. **a**. Two-step ACP to pattern two cell types by shifting or rotating the slit structure for the second ACP application. Fluorescent image of the parallel or grid pattern of normal human lung fibroblasts (NHLFs) stained red (cell seeding density 1M cells/ml) and green (1M cells/ml) patterned using ACP with a slit structure in a two step-process. The second ACP was applied after 30 min after the first application to allow cells to attach to substrate. The fluorescent image of a pattern consists of vertically aligned NHLFs stained red against lines of NHLFs stained in green. Acoustic pressure 0.2 MPa, ACP application for 10 s. **b**. Two-step ACP to generate cluster of cells using a 2-step ACP where the second ACP was applied immediately after the first application but with the slit structure rotated for 90-degree. Bright field image showing the cluster of NHLFs (cell seeding density 1M cells/ml) using the 2-step ACP approach. The second ACP was applied immediately after the first application before cell attachment. Acoustic pressure 0.2 MPa, ACP application for 10 s. Experiment was repeated independently 3 times with similar results.

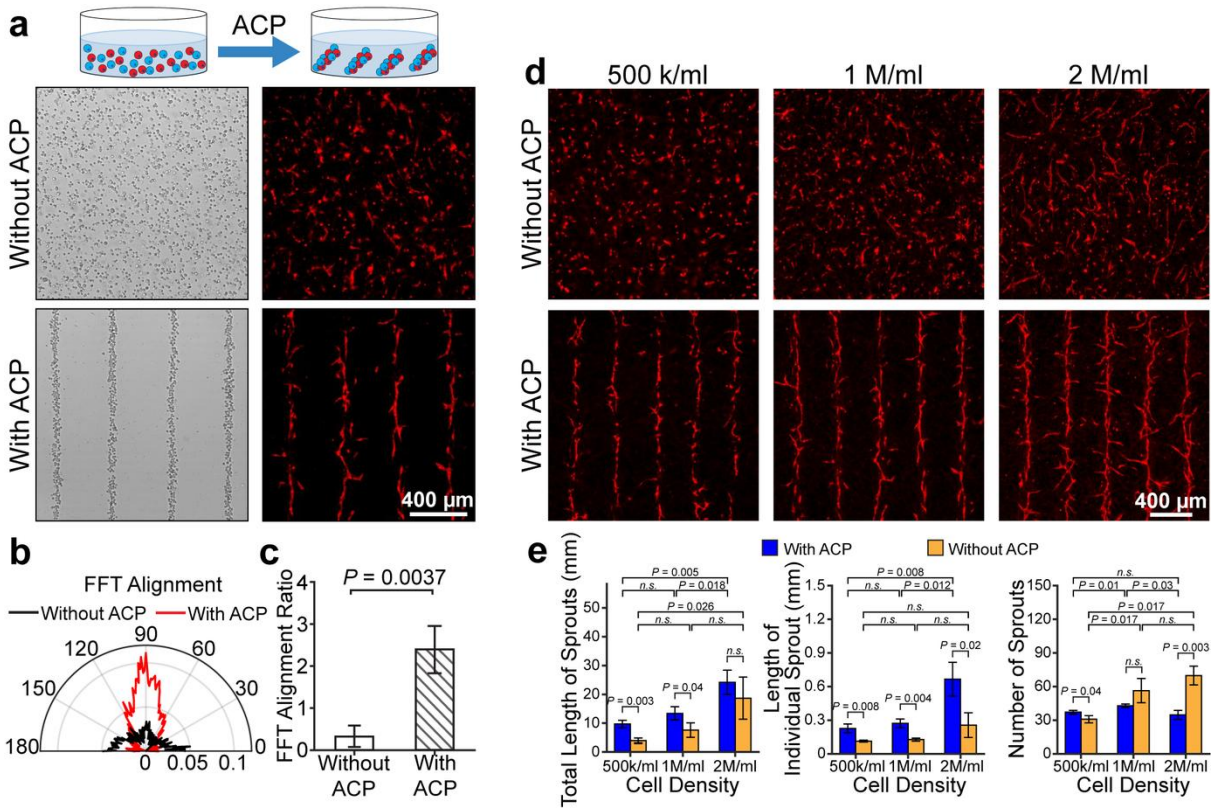

Figure S13. **a**. Patterning of mixture of human umbilical vein endothelial cells (HUVECs) and NHLFs (1:1) using ACP with a slit structure. Left: bright field images of cells with and without ACP. Right: fluorescent images of rhodamine-labeled UEA-I staining identifying HUVECs on day 5. Experiment was repeated independently 3 times with similar results. **b**,**c**. Alignment of angiogenic sprouts within the line patterns determined by 2D FFT of UEA-I images on day 5 with and without patterning by ACP respectively. Cell seeding density 1 M cells/mL. **d**. Patterning of mixture of HUVECs and NHLFs (1:1) at different cell seeding densities. Experiment was repeated independently 3 times with similar results. **e.** The total length of sprouts, length of individual sprout, and the number of sprouts in the field of view with and without application of ACP respectively. N = 3 for all groups. Scale bars: 0.4 mm. ACP: application duration 10 s, acoustic pressure of 0.12 MPa, frequency 1.68 MHz; slit structure: slit period 0.8 mm, slit width 0.4 mm. Five images per construct were taken over a 50 μm depth (10 slices at 5 μm thick) at 4X magnification. Slices were superimposed using maximum intensity z-projection and length of sprouts was quantified using the Angiogenesis Tube Formation module in Metamorph Premier (Molecular Devices). n.s. represents $p > 0.05$.

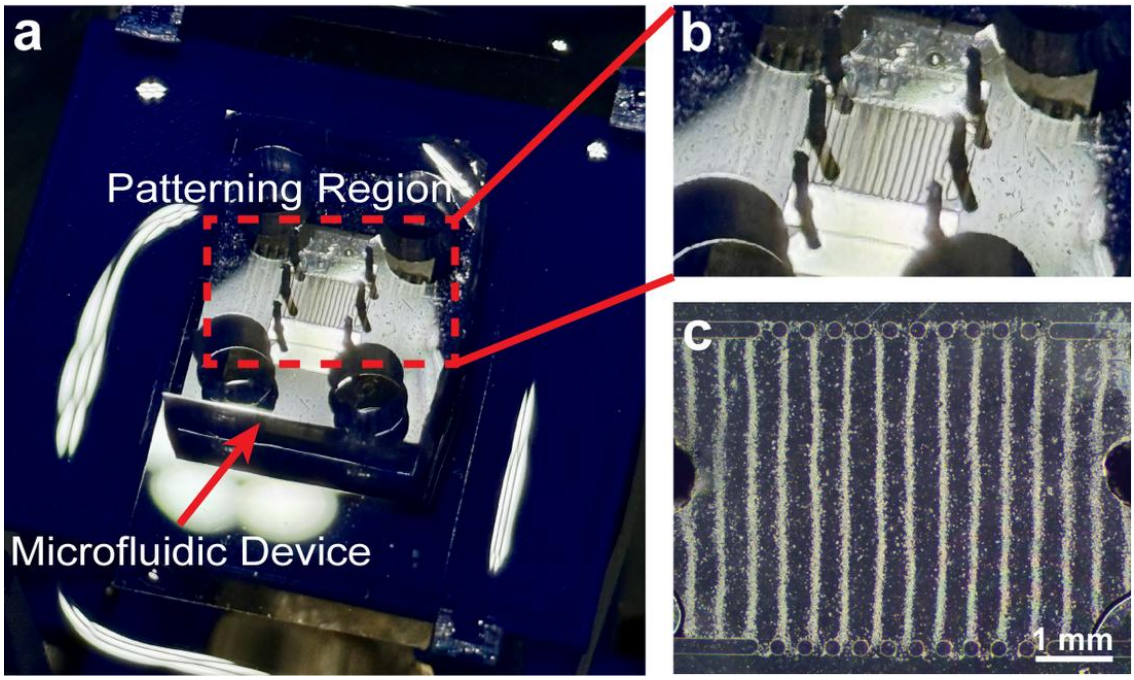

Figure S14. **a**, **b.** Photograph of the ACP setup showing ACP-generated neural tube-like structures (NTLSs) inside a microfluidic device. **c**. Bright-field image of the patterned cells immediately after ACP application (30 s). Experiment was repeated independently 3 times with similar results.

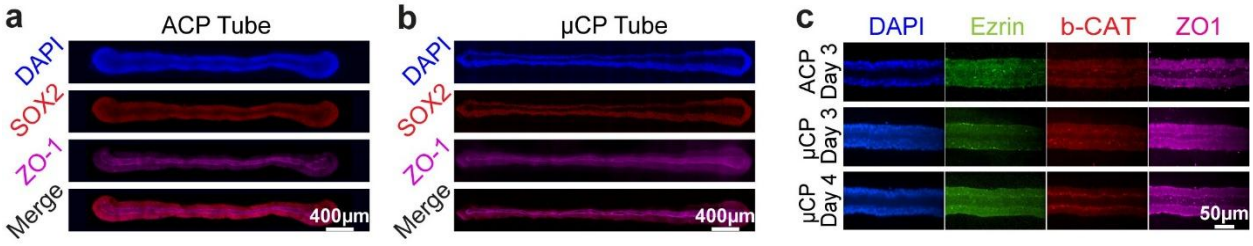

Figure S15. **a**. Representative confocal images of a tubule structure on day 3 formed from patterned hPSCs using ACP with a slit plate structure. **b**. Representative confocal images of a tubule structure on day 4 formed from patterned hPSCs using µCP. **c**. Representative confocal images showing close-up views of NTLSs patterned by ACP or µCP, staining of cell-cell contacts and apico-basal polarity. Experiment was repeated independently 3 times with similar results.

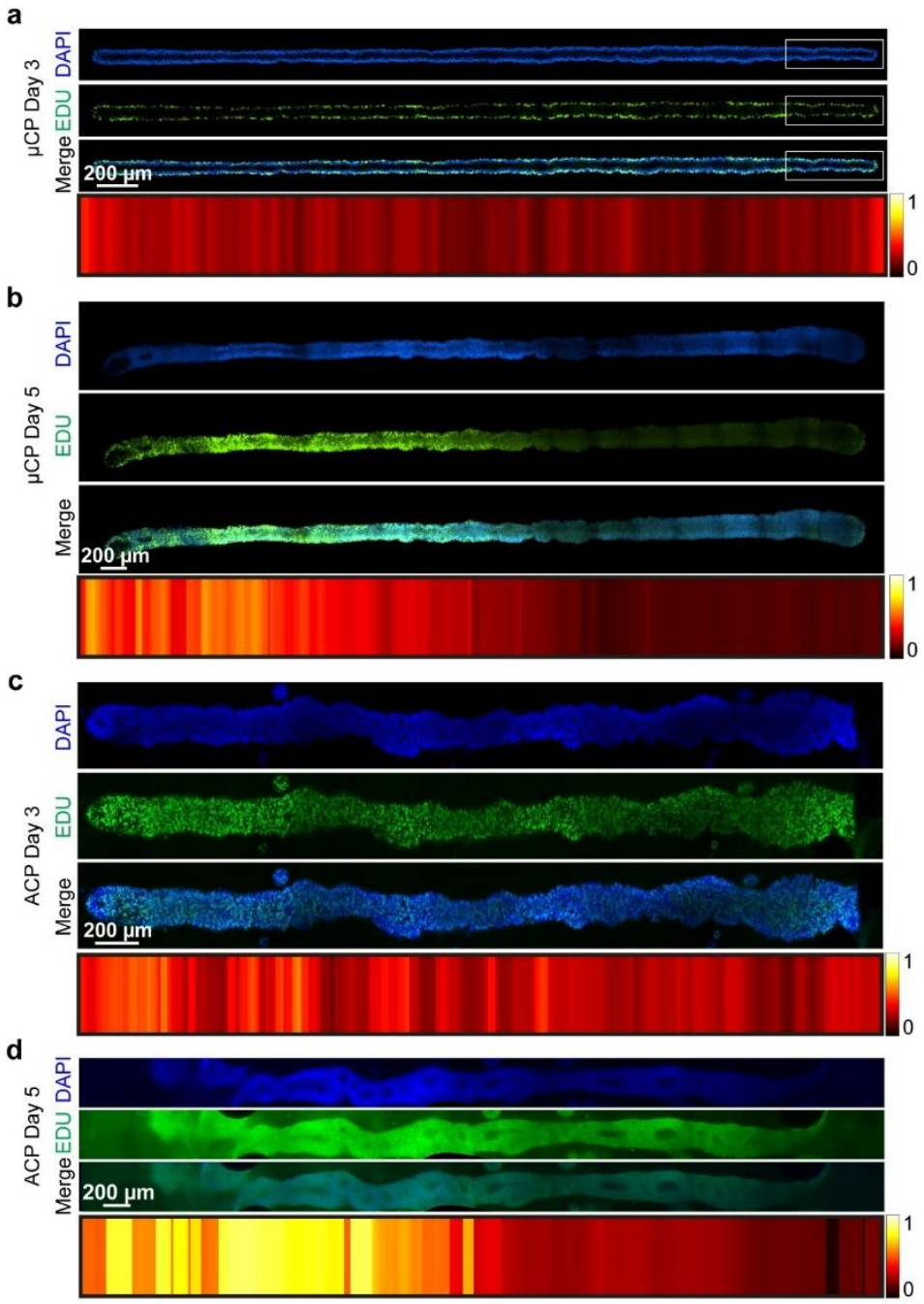

Figure S16. EdU staining of ACP- and μCP-patterned NTLSs with close-up views of the caudal region. Representative confocal images of μCP NTLSs on days 3 (**a**) and 5 (**b**), and of ACP NTLSs on days 3 (**c**) and 5 (**d**). Experiment was repeated independently 3 times with similar results.

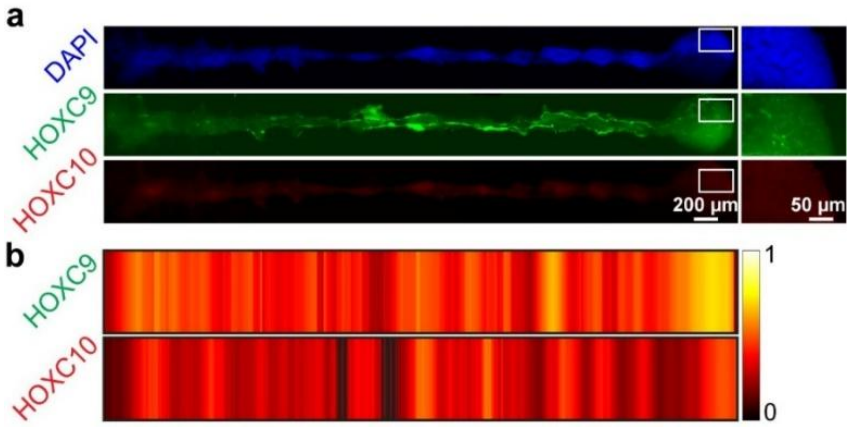

Figure S17. a. Immunofluorescence images of HOXC9 and HOXC10 expression of a representative NTLS derived from µCP-generated hPSC strips (length 6 mm) on day 14. Experiment was repeated independently 3 times with similar results. **b**. Heatmap of HOXC9 and HOXC10 expression generated from three NTLS derived from µCP-generated hPSC strips (length 6 mm) on day 14.

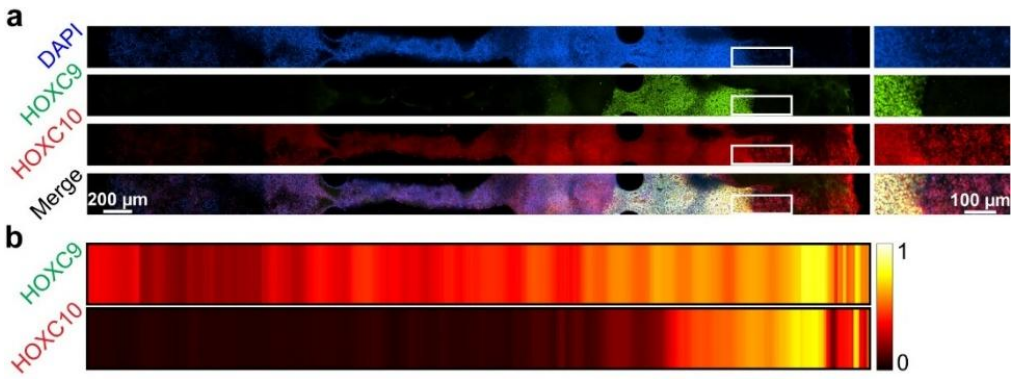

Figure S18. **a**. Immunostaining images of HOXC9 and HOXC10 expression on day 14 in a representative NTLS generated from ACP patterned hPSC strip colonies of 2 mm length. Experiment was repeated independently 3 times with similar results. **b**. Heatmap of HOXC9 and HOXC10 expression generated from three NTLS derived from ACP-generated hPSC strips (length 2 mm) on day 14.

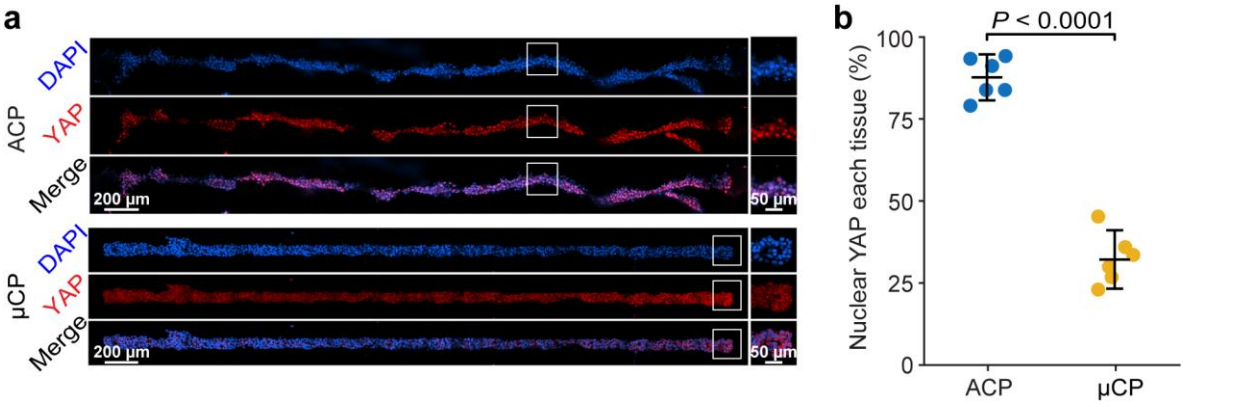

Figure S19. **a**. Representative confocal images of a tubule structure on day 1 formed from patterned hPSCs using ACP and a tubule structure on day 4 formed from patterned hPSCs using μCP. Experiment was repeated independently 3 times with similar results. **b**. Percentage of cells with positive nuclear YAP in each in ACP- and μCP-generated tubule structures.

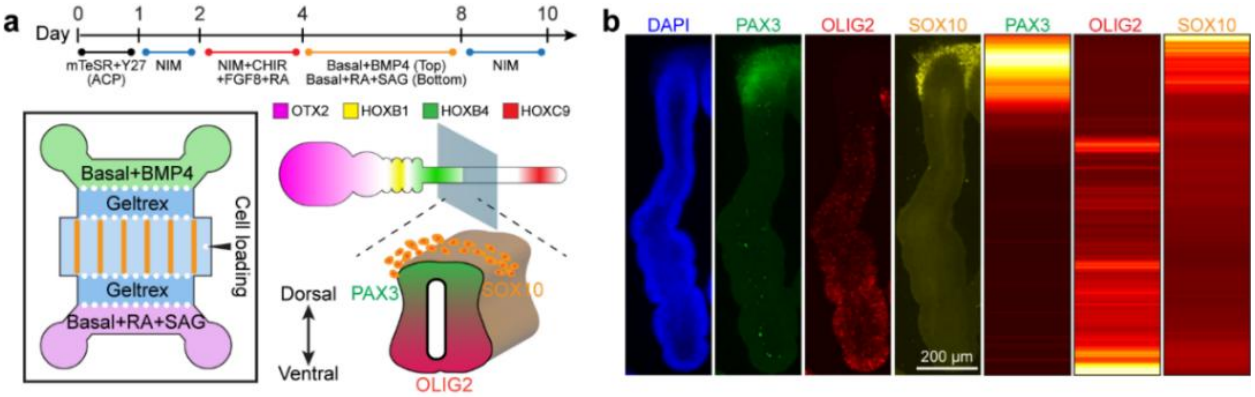

Figure S20. a. Protocol and schematics for generating dorsal-ventral (D-V) patterning of NTLS formed from patterned hPSCs using ACP (with a slit structure) within a microfluidic device to control morphogen gradient. **b**. Confocal images and heat maps of immunostaining of DAPI, PAX3, OLIG2, and SOX10 in NTLS respectively. Number of experiments = 4. ACP used ultrasound pressure of 0.2 MPa and application time is 10 s. Cell seeding density 4 M cells/ml. Experiment was repeated independently 3 times with similar results.

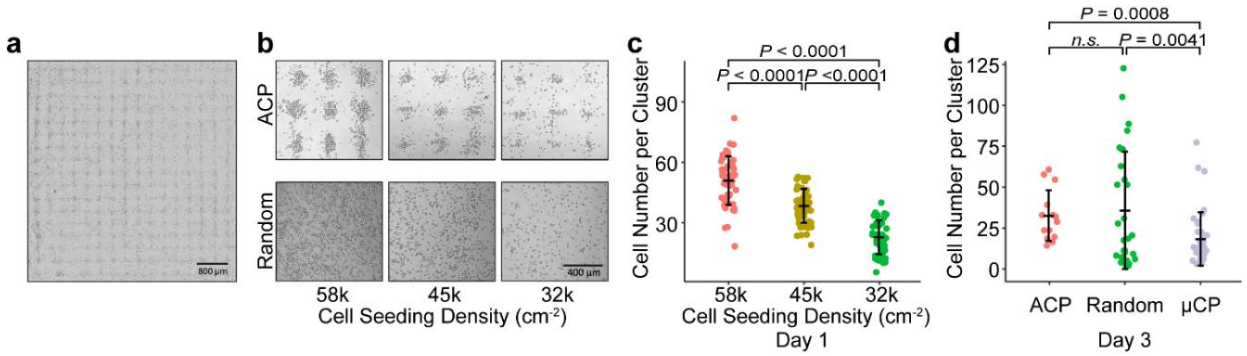

Figure S21. **a**. Global view of ACP-generated hPSC clusters on glass. Two-step ACP application was used with a slit structure. Experiment was repeated independently 3 times with similar results. **b**. Enlarged views of ACP-generated hPSC clusters (top) and randomly distributed hPSCs (bottom) at different cell seeding density. **c**. Cell number per cluster generated by ACP on day 0 at different cell seeding density. **d**. Cell number per cluster by ACP, randomly seeded hPSCs, and μCP on glass (day 3) respectively. N= 3 independent experiments.

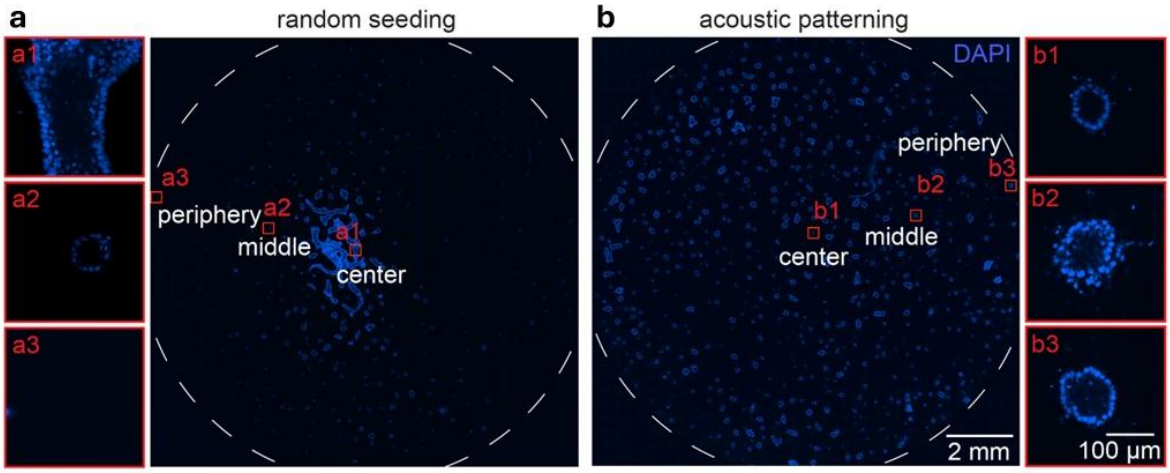

Figure S22. Example confocal image of the entire petri dish showing colonies formed from randomly distributed hPSCs (**a**) or using ACP (**b**). Inset: a1, a2, and a3 and b1, b2, and b3 are enlarged regions near the center, middle, and periphery area indicated in (**a**) and (**b**) respectively. Samples were cultured under 3D culture condition and imaged on day 6. Experiment was repeated independently 3 times with similar results.

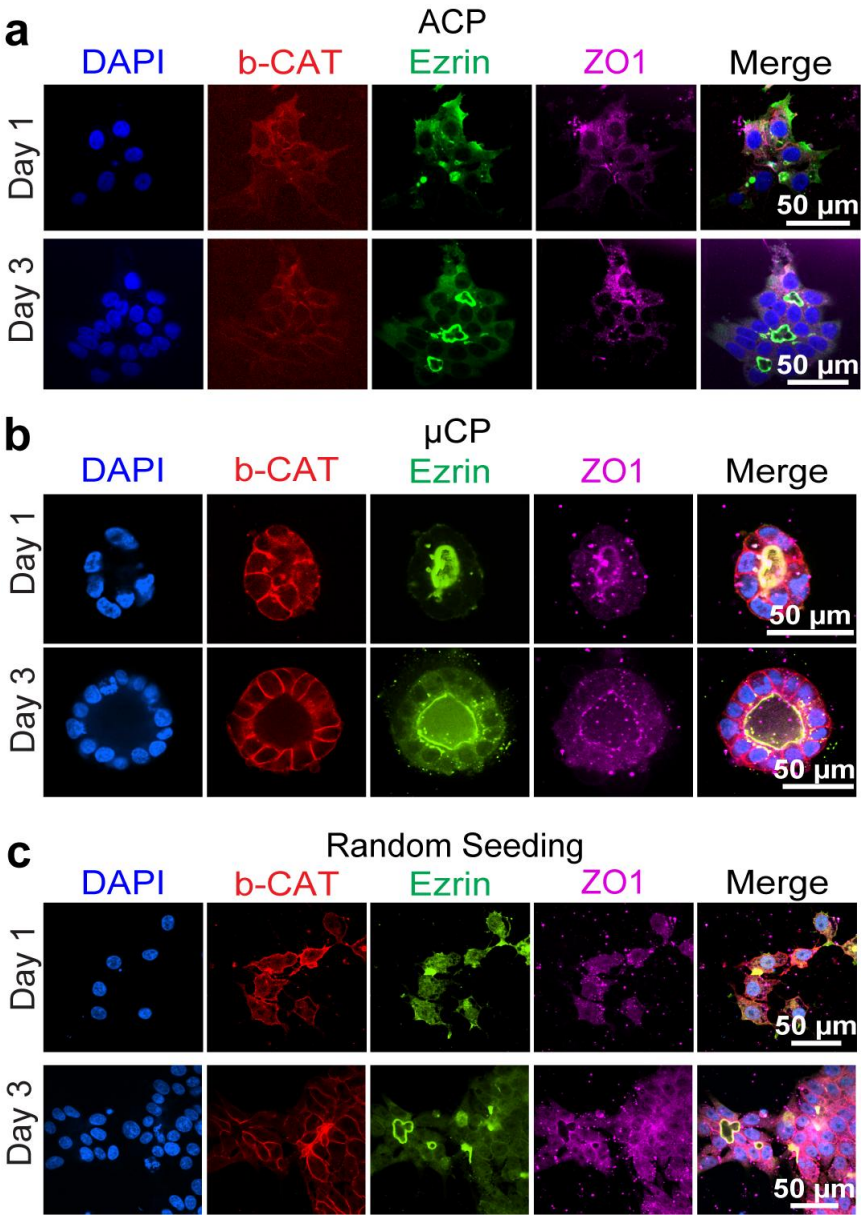

Figure S23. **a-c**. Immunostaining of cell adhesion markers β-catenin, ezrin, ZO-1 in ACP- (**a**), μCP- (**b**), and randomly seeded (**c**) hPSC clusters formed on glass substrates and cultured in 2D. Experiment was repeated independently 3 times with similar results.

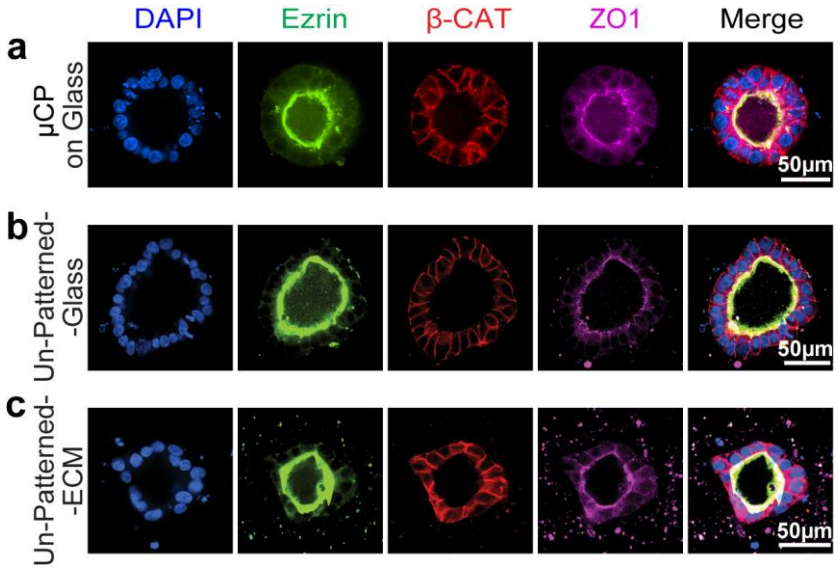

Figure S24. Representative confocal immunofluorescence images of 3D cyst structures (day 4) generated from μCP-patterned hPSCs on glass (**a**) and randomly seeded hPSCs on glass (**b**) and ECM bed (**c**). Experiment was repeated independently 3 times with similar results.

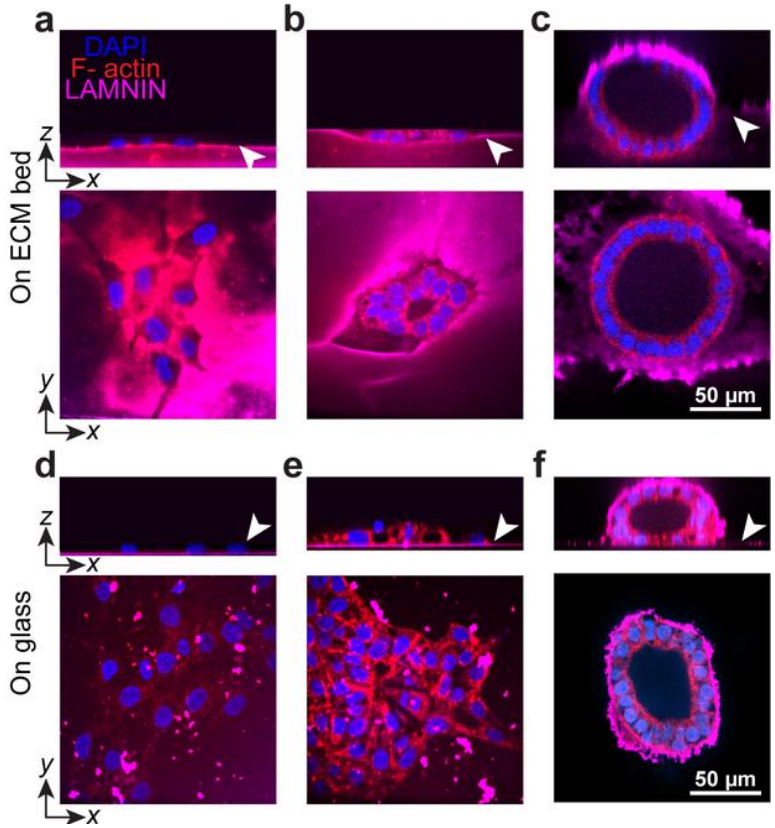

Figure S25. Epiblast-like structures formed from ACP generated hPSC clusters on a solidified Geltrex layer (ECM bed) or glass substrate. Cells were stained with DAPI (blue) and ECM (Geltrex) stained with F-actin and Laminin (pink). **a**. Confocal images showing the side view (top) and top

view (bottom) of ACP-generated hPSC cluster on ECM bed on day 1. **b.** Confocal images showing the side view (top) and top view (bottom) of ACP-generated hPSC cluster cultured using a 2D culture protocol (mTeSR only) on ECM bed on day 4. **c.** Confocal images showing the side view (top) and top view (bottom) of ACP-generated hPSC cluster cultured using a 3D culture protocol (4% Geltrex) on ECM bed on day 4. White arrowheads indicate the surface of the ECM bed in (**a - c)**. **d**. Confocal images showing the side view (top) and top view (bottom) of ACP-generated hPSC cluster on glass on day 1. **e.** Confocal images showing the side view (top) and top view (bottom) of ACP-generated hPSC cluster cultured using a 2D culture protocol (mTeSR only) on glass on day 4. **f.** Confocal images showing the side view (top) and top view (bottom) of ACP-generated cluster cultured using a 3D culture protocol (4% Geltrex) on glass on day 4. White arrowheads indicate the surface of the glass slide in (**d** – **f**). Experiment was repeated independently 3 times with similar results.

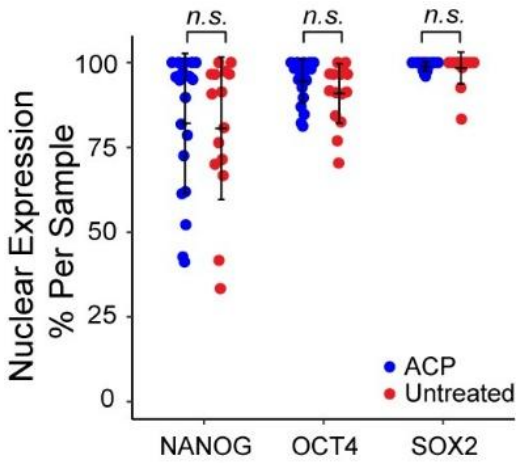

Figure S26. Percentage of cells per cyst with nuclear expression of NANOG, OCT4, and SOX2 on day 4 respectively determined from immunostaining of samples. ACP group: cysts were formed from ACP-treated hPSCs that were subsequently cultured in random seeding condition on glass. Untreated group: cysts formed from un-patterned hPSCs in random seeding condition without ACP on glass substrate.

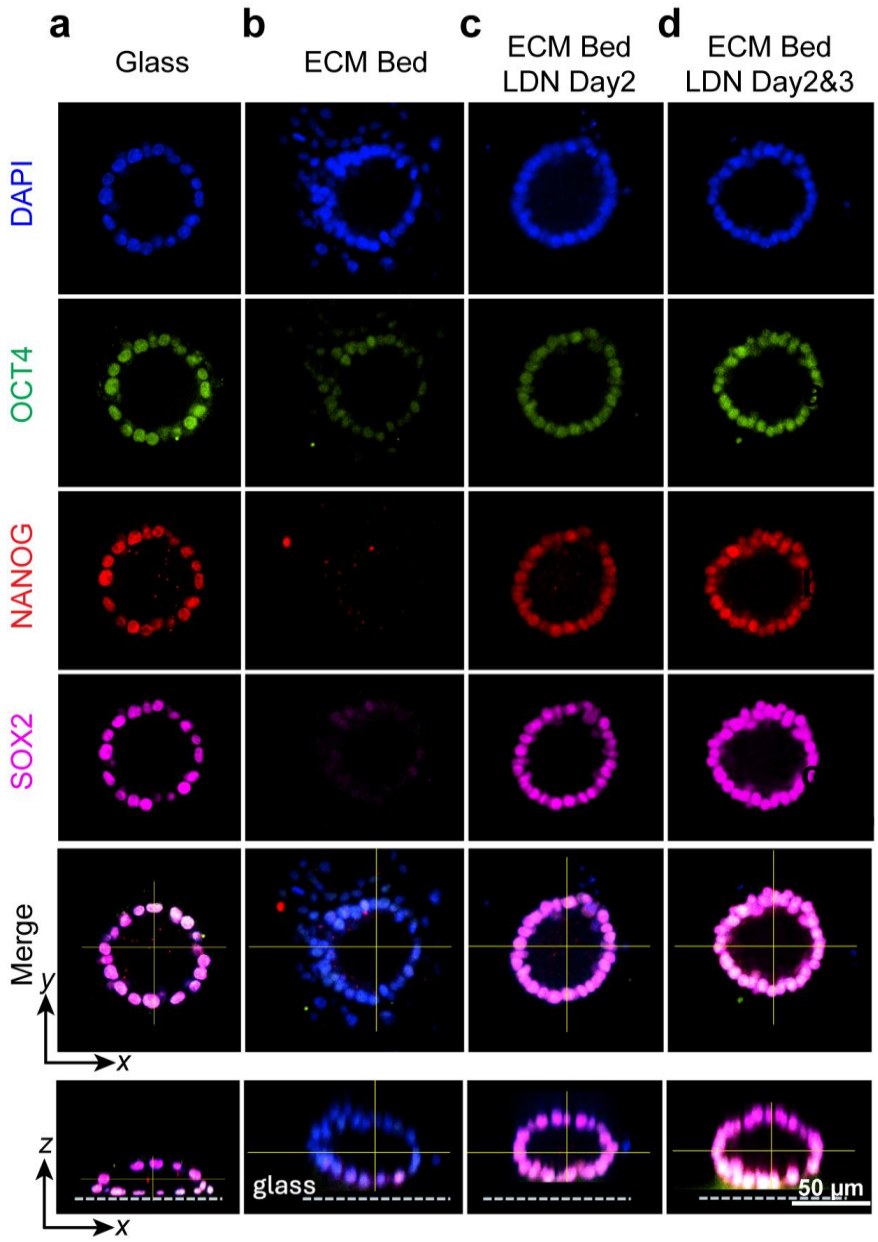

Figure S27. Confocal images showing immunostaining of ACP-generated cysts on glass (**a**) and on ECM bed (**b**) with standard culture or treated using bone morphogenetic protein (BMP) inhibitor LDN193189 (LDN) on day 2 (**c**) or on both day 2 and day 3 (**d**). Samples were imaged on Day 4. Experiment was repeated independently 3 times with similar results. Scale bar: 50 µm.

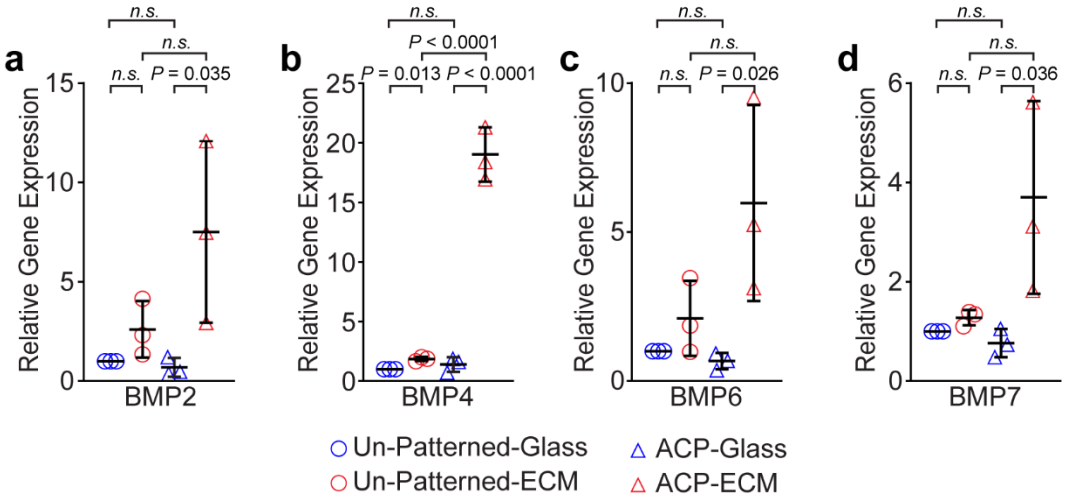

Figure S28. qRT-PCR results of expression levels BMP2 (**a**), BMP4 (**b**), BMP6 (**c**), and BMP7 (**d**) of cysts on day 4 for the following four groups: cysts formed from spontaneously clustering of hPSCs on glass (control glass, blue circles) or on ECM (control ECM, red circles), cysts formed from ACP-generated hPSC clusters on ECM (patterned ECM, red triangles) or glass substrate (Patterned glass, red triangles) respectively on day 4. Data normalized against GAPDH and the control-glass group. n = 3 for all groups.

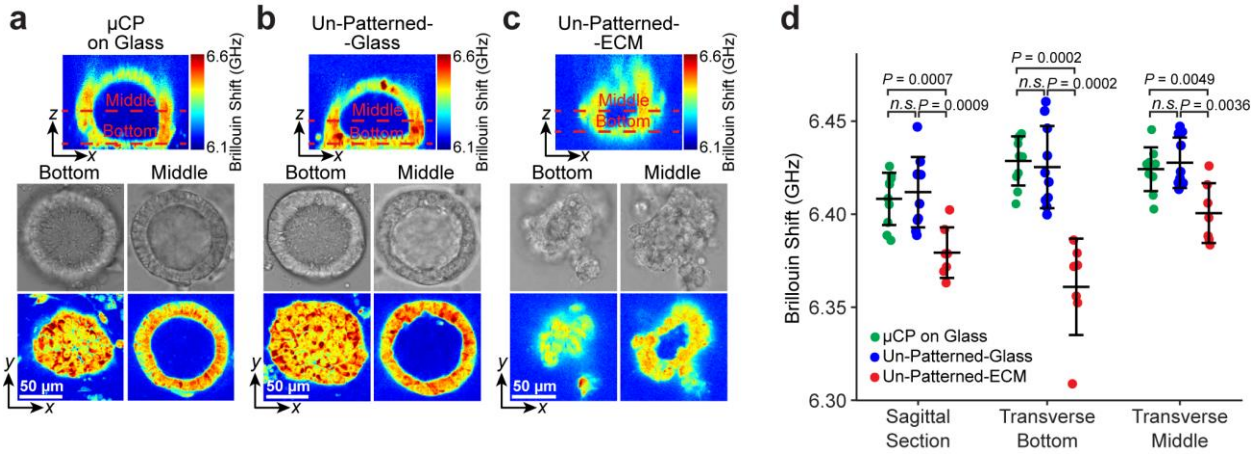

Figure S29. **a-c**. Brillouin imaging of cysts formed from patterned hPSCs on glass using μCP (**a**), and from randomly seeded hPSC on glass (**b**) and ECM bed (**c**) respectively. Top: Example images of Brillouin shift of cysts in the sagittal plane; middle and bottom: Transverse plane bright-field images and Brillouin shift images at the bottom and middle plane from the cysts in **a**–**c** respectively. Experiment was repeated independently 3 times with similar results. **d**. Quantification of Brillouin shift in cysts generated on glass using μCP, randomly seeded hPSCs on glass and on ECM bed in the sagittal plane, transverse plane at the bottom and middle plane respectively.

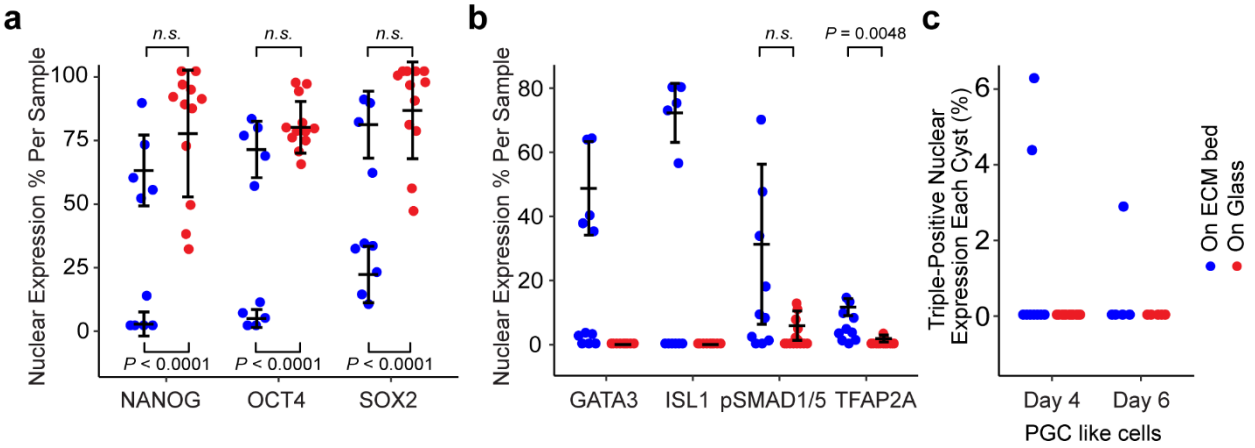

Figure S30. Control experiments of cysts formed from randomly seeded hPSCs on glass and ECM bed respectively. a. Immunofluorescence staining of pluripotency markers (OCT4, NANOG, SOX2), showing differentiation of cysts cultured on glass (red dots) or ECM bed (blue dots) on day 4. b. The percentage of Amnion markers ISL1, GATA3, TFAP2A, pSMAD1/5 in each of cysts cultured on glass (red dots) or ECM bed (blue dots) on day 4. c. The percentage of PGC-like cells with positive TFAP2C-NANOG-SOX17 co-expression in each of cysts cultured on glass (red dots) or ECM bed (blue dots) on day 4 and day 6 respectively.